

# K-shell photoionization of Nickel ions using *R*-matrix

M. C. Witthoef<sup>1,2</sup>, M. A. Bautista<sup>3</sup>, J. García<sup>3,2</sup>, T. R. Kallman<sup>2</sup>

C. Mendoza<sup>4</sup>, P. Palmeri<sup>5</sup>, and P. Quinet<sup>5,6</sup>

Received \_\_\_\_\_; accepted \_\_\_\_\_

---

<sup>1</sup>Department of Astronomy, University of Maryland, College Park, MD, USA

<sup>2</sup>NASA/Goddard Space Flight Center, Code 662, Greenbelt, MD, USA

<sup>3</sup>Department of Physics, Western Michigan University, Kalamazoo, MI, USA

<sup>4</sup>Centro de Física, Instituto Venezolano de Investigaciones Científicas (IVIC), Caracas, Venezuela

<sup>5</sup>Astrofysique et Spectroscopie, Université de Mons - UMONS, B-7000 Mons, Belgium

<sup>6</sup>INPAS, Université de Liège, B-4000 Liège, Belgium

## ABSTRACT

We present  $R$ -matrix calculations of photoabsorption and photoionization cross sections across the K edge of the Li-like to Ca-like ions stages of Ni. Level-resolved, Breit-Pauli calculations were performed for the Li-like to Na-like stages. Term-resolved calculations, which include the mass-velocity and Darwin relativistic corrections, were performed for the Mg-like to Ca-like ion stages. This data set is extended up to Fe-like Ni using the distorted wave approximation as implemented by AUTOSTRUCTURE. The  $R$ -matrix calculations include the effects of radiative and Auger dampings by means of an optical potential. The damping processes affect the absorption resonances converging to the K thresholds causing them to display symmetric profiles of constant width that smear the otherwise sharp edge at the K-shell photoionization threshold. These data are important for the modeling of features found in photoionized plasmas.

*Subject headings:* atomic data – atomic processes – line formation – X-rays:  
spectroscopy

## 1. Introduction

The K lines and edges of iron and nickel are important diagnostics in X-ray astronomy. They are in a relatively unconfused part of the X-ray spectrum ( $\sim 6\text{--}10$  keV), and they are formed over a wide range of physical conditions. This can range from cold (by X-ray standards) neutral gas at temperatures  $\leq 10^4$  K, to highly ionized gas near  $10^8$  K. Their energy and shape give information about the ionization and kinematics in the gas. The strengths of emission features, such as K fluorescence lines, constrain the amount of emitting gas and the elemental abundances, while the strengths of absorption edges constrain the column densities along the line of sight to the background X-ray source. Iron K lines and edges have been studied by many existing and past X-ray astronomy instruments. They have provided insights into diverse topics such as elemental abundances in clusters of galaxies (Serlemitsos et al. 1977), the spin of black holes (Brenneman et al. 2011; McClintock et al. 2011), and the geometry of stellar flares (Testa et al. 2008). Nickel features have not yet been used to the same extent, owing to the fact that they are weaker by a factor  $\sim 10$  from the typical Ni/Fe abundance ratio, and to the fact that many detectors have collecting areas which decrease rapidly above 7 keV. Nonetheless, Nickel has been detected in systems ranging from black hole X-ray binaries (Miller et al. 2006; Kallman et al. 2009), clusters of galaxies (Tamura et al. 2009), the center of our galaxy (Koyama 2011), and supernova remnants (Tamagawa 2010). Further impetus for calculations of the spectra of nickel comes from the *Astro-H* satellite, which will result in the most sensitive observations to date of objects at energies containing K features of nickel. This is because of both the relatively large sensitivity at the energy of the nickel K lines and edges (7.2 – 10.7 keV), and because of its spectral resolution, which will exceed that of previous experiments at energies above 3 keV.

Over the last several years, our group has worked on providing accurate K-shell

atomic data for all ions of astrophysical interest. We have calculated energy levels, wavelengths, Einstein  $A$ -coefficients, Auger rates, and photoabsorption/ionization cross sections. Complete data sets have been computed for all ion stages of Fe (Bautista et al. 2003; Palmeri et al. 2003a,b; Mendoza et al. 2004; Bautista et al. 2004; Kallman et al. 2004), O (García et al. 2005), N (García et al. 2009), as well as Ne, Mg, Si, S, Ar, and Ca (Palmeri et al. 2008a; Witthoeft et al. 2009, 2011). There has also been recent work on the C sequence by Hasoglu et al. (2010) using similar techniques.

The data we present in this work are important both for their direct effect on observed astrophysical X-ray spectra via absorption features, and also through their effect on ionization balance calculations, which in turn affects many of the observables from these elements. In particular, it is the detailed resonance and edge structure, missing in previous calculations, which is most important.

There have been a large number of calculations for these systems going back to the 1920's, but they are confined to the non-resonant background and few span the K edge region. For the ions considered in this work, there is good agreement between our results and the background cross section both above and below the K edge characterized by the fits of Verner & Yakovlev (1995). Laboratory measurements have been mainly confined to neutral systems for photon energies beyond the K edge. A comprehensive assessment and fitting of measurements has been performed by Veigele (1973).

There has been recent progress measuring the resonance structure near the K edge of Li-like systems:  $C^{3+}$  (Müller et al. 2009) and  $B^{2+}$  (Müller et al. 2010), as well as Be-like  $C^{2+}$  (Scully et al. 2005).  $R$ -matrix calculations performed as part of those works are in good agreement with the measurements apart from small discrepancies in some resonance positions and heights. With the advances of free electron lasers to produce X-rays (Kanter et al. 2006), we expect it will be possible over the next several years to

perform similar experiments for the K-shell absorption by heavier species. However, such measurements for Ni are not yet available.

## 2. Numerical methods

The  $R$ -matrix method employed here is the same as previous K-shell calculations in this series, c.f. Bautista et al. (2003). The  $R$ -matrix method is based on the close-coupling approximation of Burke & Seaton (1971), which is solved numerically following Burke et al. (1971); Berrington et al. (1974, 1978, 1987).

As in our previous calculations, the effect of radiative and spectator Auger decay on resonances is included using the optical potential of Gorczyca & Badnell (1996, 2000). Here, the resonance energy with respect to the threshold acquires an imaginary component which is the sum of the radiative and Auger widths of the core. The radiative widths are computed within the  $R$ -matrix calculations following the prescription given by Robicheaux et al. (1995). The Auger widths are taken from the relativistic Hartree-Fock calculations of Palmeri et al. (2008b). These effects are referred to as radiative and Auger damping since they cause resonances in the photoionization cross section to become smaller in area. The damping also makes it necessary to calculate both the photoabsorption and photoionization cross sections since not every absorbed photon will result in a photoelectron.

We use the  $R$ -matrix computer package of Berrington et al. (1995) for the inner region calculation and the asymptotic region code STGBF0DAMP<sup>1</sup> (Gorczyca & Badnell 1996) is used to compute the photoabsorption and photoionization cross sections including the effects of damping.

---

<sup>1</sup><http://amdpp.phys.strath.ac.uk/tamoc/code.html>

For the Li-like to Ne-like ions, our target expansion includes all states in the configurations:  $1s^2 2l^w$  and  $1s 2l^{w+1}$  where  $w = 0$  for Li-like and  $w = 7$  for Ne-like. Note that the target refers to the final state which has one fewer electron than the initial state; thus the Ne-like case having a 9-electron target. For the remaining ions, we must include  $n = 3$  orbitals. The included configurations are  $1s^2 2l^8 3l^w$ ,  $1s^2 2l^8 3l^{w-1} 3d$ ,  $1s^2 2l^7 3l^{w+1}$ , and  $1s 2l^8 3l^{w+1}$  where  $l$  is restricted to s and p electrons. We only include 3d excited states from the valence configuration to improve the atomic structure. We have tested the addition of 3d configurations in the L- and K-hole states for Mg-like and Ar-like Ni and have found the following differences. First, the  $K\beta$  resonances are shifted by a couple eV which is within the uncertainty of the calculation. This difference in the resonance positions decreases approaching the K edge. Secondly, the larger calculation has a few additional resonances, but these are small and disappear when the cross section is convolved with a resolution reflective of current X-ray detectors. Therefore, we are confident in omitting the additional 3d configurations for all of the present calculations.

We include enough continuum basis orbitals to span from threshold to at least four times the energy of the K edge. This choice gives reliable cross sections up to at least twice the energy of the K edge. Partial photoionization and total photoionization/absorption cross sections are calculated from all states in the ground configuration of the parent ion.

The close-coupling expansion is small enough for the Li-like to Na-like ions to allow for fully level-resolved, Breit-Pauli (BPRM) calculations to be carried out. The number of fine-structure levels for the other ions quickly becomes too large for the computational resources available, so we revert to  $LS$ -coupling for the remaining ions. The mass-velocity and Darwin terms are still included in these calculations which greatly improve the target energies. Wave functions are obtained using AUTOSTRUCTURE (Badnell 1986, 1997) where the level/term energies have been adjusted to match those in the NIST database

(Ralchenko et al. 2008) when possible, otherwise we match our energies to those calculations by Palmeri et al. (2008b). Some levels in our target expansion are not listed by either of the above sources. For such valence and L-vacancy states, we use our AUTOSTRUCTURE energies unshifted. For the unlisted K-hole states, we shift our energies to match the average difference between the K-hole states appearing in both our target and Palmeri et al. (2008b). This last shift is approximately 25 eV (0.3%) for the Mg-like to Ca-like ions. The resulting cross sections are shifted in energy so that the ionization threshold matches NIST. This final shift brings the K edge thresholds within 0.5% of those given by Palmeri et al. (2008b).

Cross sections for Sc-like to Fe-like Ni are calculated using the distorted wave method as implemented by AUTOSTRUCTURE. These calculations use the same configuration expansion as the  $R$ -matrix calculations with the exception of Fe-like Ni which includes the  $3d^6 4\ell$  ( $\ell = 0, 1, 2$ ) configurations. Resonances are included using the isolated resonance approximation up to  $n = 20$ . These calculations are performed in  $LS$  coupling and the energies are shifted so that the location of the K edge matches Palmeri et al. (2008b). The background cross section is calculated up to 13.6 keV while resonances are calculated only near the K edge. AUTOSTRUCTURE can construct wave functions from either the  $N$ -electron target orbitals or the  $(N + 1)$ -electron parent orbitals. The difference in the cross sections using both sets of wave functions gives an idea of the uncertainty of this method. The wave functions are composed of relaxed (non-orthogonal) orbitals. Since we do not attempt to take radiation or Auger dampings into account, we only report total photoabsorption cross sections which are convolved with a Gaussian profile. The width of the Gaussian is  $\Delta E/E = 10^{-3}$  which is representative of currently deployed X-ray detectors. Calculations for Ni I and Ni II are more involved, so we leave these for future work.

### 3. Results

The cross sections reported here contain many of the same features shown in the results from our previous calculations. Inclusion of radiation and Auger damping broadens resonances near the K edge and makes them more symmetric. The damping is also important in distinguishing the absorption and ionization cross sections. In Figure 1, we show these cross sections for the  $^1S_0$  ground state of Ne-like Ni. As there are no  $K\alpha$  resonances for Ne-like ions, the first resonance is  $K\beta$ . The effect of damping is observed in both the photoionization and photoabsorption resonances. In the former, the heights of the resonances are greatly diminished, especially as the photon energy approaches the K edge due to the dominance of the spectator Auger process. For photoabsorption, both radiation and Auger damping broaden the resonances and make them more symmetric.

For this simple system, one would expect a single resonance for each Rydberg  $n$ -shell, however, the  $K\beta$  resonance has two peaks in our results. This represents the breakdown of  $LS$  coupling at large  $Z$ . For low- $Z$  ions, the  $2p^6\ ^1S_0$  ground state goes to the  $1s\ 2s^2\ 2p^6\ 3p\ ^1P_1$  state. At high  $Z$ , the total spin is no longer a conserved quantity, making the  $^3P_1$  state accessible leading to the second  $K\beta$  peak. For the  $n > 3$  resonances,  $LS$  coupling remains a good description for a Rydberg electron attached to a core, so only a single resonance is found. The appearance of the second  $K\beta$  resonance as  $Z$  increases is demonstrated in Fig 2 where we show the  $K\beta$  resonance for six Ne-like ions from  $Z = 12$  to 28 using data from Witthoef et al. (2009). The separation of the  $K\beta$  resonances for Ne-like Ni is approximately 5 eV which should be detectable in the next generation of X-ray observatories, such as *Astro-H*.

In Figure 3, we show the background cross sections at fixed photon energies above and below the K edge (at 10.9 keV and 6.8 keV, respectively) for all Ni ions included in this work. For comparison, we also include the results from Verner & Yakovlev (1995). Both

results agree within a few percent along the whole iso-nuclear sequence. The background below the K edge steadily increases until the  $n = 2$  shell is filled (Ne-like), where the background becomes constant. This is because the background is dominated by the L-shell cross section and the 2s and 2p electron wave functions are not affected much by the addition of  $n = 3$  electrons. For the same reason, but for 1s electrons, the background cross section above the K edge is relatively constant beyond He-like Ni.

Resonances in the cross section are often quite narrow, even when Auger damping is included, requiring tens of thousands of energy points to resolve all the features. In modeling codes, this amount of data is cumbersome, so we convolve our cross sections with a Gaussian profile having a width of  $\Delta E/E = 10^{-4}$ . An example of the convolution is shown in Figure 4 for Be-like Ni for both photoabsorption (top panel) and photoionization (bottom panel). The convolved results demonstrate the strength of damping as the resonant contribution to the cross section for photoionization is nearly gone at the K edge. For photoabsorption, on the other hand, the resonances converge onto the K edge, causing the perceived edge in the convolved results to occur at a smaller energy; this is known as the smearing of the K edge in absorption spectra.

As part of an effort to calculate recombination rate coefficients, Nahar (2005) performed a Breit-Pauli  $R$ -matrix calculation for Li-like Ni with energies extending beyond the K edge. We are in good agreement with those results for the ground state with respect to the resonance positions and the location of the K edge. However, there is some disagreement with the background cross section in the vicinity of the edge. In Figure 5 the present results are compared with the results of Nahar (2005) and Verner & Yakovlev (1995). Below the edge, we find fair agreement, the background of Nahar being about 10% higher than the present results, while above the edge, the Nahar background is nearly 30% lower. The disagreement above the edge disappears entirely above a photon energy of 11.5 keV. The

background from the present results are in excellent agreement with Verner & Yakovlev (1995) at all energies, although their K edge position is about 50 eV lower than that calculated by ourselves and Nahar (2005).

We find larger differences with Nahar (2005) in the amount of resonant enhancement. This appears to be due to the higher energy resolution used in our calculation. Unlike the rest of the ions covered in this work, the Li-like system does not have a spectator Auger process which would significantly damp the narrow photoionization resonances near the K edge, as observed in Figure 4. Instead, there is a large number of extremely narrow, yet strong, resonances which need to be fully resolved to account for their area. Nahar (2005) uses about 20000 energy points to map out the cross section. For the present calculation, we use the technique described in Witthoeft et al. (2009) which automatically identifies the location of each resonance and adds enough energy points to fully resolve it. Even with the efficiency of this approach, over a half million points were required to properly resolve all resonance features. To illustrate the strength of the narrow resonances near the K edge, we show in the inset of Figure 5 the resonance structure in a narrow energy range. The difference between the calculations becomes particularly apparent when comparing convolved cross sections. Using a Gaussian width of  $\Delta E/E = 10^{-3}$ , we find that the Nahar (2005)  $K\alpha$  resonances are about 5 times weaker than in the present results; near the K edge, the difference is nearly an order of magnitude. These differences are expected to be important for spectral modeling of X-ray plasmas.

Total photoionization cross sections have been calculated using AUTOSTRUCTURE for Ar-like to Fe-like Ni. The first three ions of this sequence have also been calculated using *R*-matrix which allows for a comparison of the methods. In Figure 6, we compare the present *R*-matrix results with two sets of AUTOSTRUCTURE results using wave functions constructed from target or parent orbitals. All data have been convolved with a

Gaussian using a width of  $\Delta E/E = 10^{-3}$ . Also shown are the direct photoionization cross sections of Verner & Yakovlev (1995). The AUTOSTRUCTURE results have been shifted in energy ( $\sim 25$  eV) so that the K edge is in agreement with Palmeri et al. (2008b). The Verner & Yakovlev (1995) results are unshifted and a disagreement of  $\sim 50$  eV in the edge position is observed. The background cross sections above and below the K edge from the  $R$ -matrix and both AUTOSTRUCTURE calculations are in good agreement. The background of Verner & Yakovlev (1995), on the other hand, is about 10% lower than the  $R$ -matrix results just above the K edge, but comes into good agreement by 10 keV. There is some disagreement in the position and height of the first resonance ( $K\gamma$ ) which is due to the relaxation effects on the orbitals in the AUTOSTRUCTURE calculations which are not included in  $R$ -matrix. This disagreement becomes smaller for the rest of the resonance series. If we were to use orthogonal orbitals in the AUTOSTRUCTURE calculations, the agreement of the resonance positions with  $R$ -matrix would improve, but the discrepancy of the resonance heights remains. Since the AUTOSTRUCTURE calculation using the target orbitals gives better agreement with  $R$ -matrix than that using parent orbitals (which is also true for Ar-like and K-like Ni), we continue to use target orbitals for the Sc-like to Fe-like AUTOSTRUCTURE calculations. Clearly these systems would benefit from future  $R$ -matrix calculations, but in the meantime, the AUTOSTRUCTURE data provide an improvement over previous calculations where resonances are neglected entirely.

By default, AUTOSTRUCTURE calculates cross sections using the length gauge. This begins to fail numerically at high energies above the K edge and the velocity gauge is more accurate. We take cross sections calculated using the length-gauge at energies below the K edge and the velocity gauge results for energies above the edge. This method yields a background cross section in good agreement with the  $R$ -matrix results for Ar-like to Ca-like Ni, and is applied to the other systems.

Data from this work are to be used in the XSTAR code (Kallman & Bautista 2001; Bautista & Kallman 2001) for modeling photoionized plasmas. To prepare for this application, we need to reduce the number of data points from thousands to hundreds. In addition to convolution (as described earlier), we remove unnecessary data points from each data set in the following manner. Points which lie on a straight line between the two adjacent points within 1% are removed. This test is repeated over the entire cross section until no more points are removed. Using this process, we can decrease the number of points in the cross section data from several thousand to a few hundred, yet still maintain good accuracy with linear interpolation. The convolved cross sections are not included with this paper, but are available by a request to MCW, XSTAR<sup>2</sup>, or the Universal Atomic Database<sup>3</sup>. The raw cross sections are available as electronic tables attached to this work.

The energy range of all datasets in the present work begin at the valence-shell threshold. However, as we are only focused on the resonance features near the K edge, we have not attempted to fully resolve the resonances in the region of the L edge.

#### 4. Summary and Conclusions

Total photoabsorption and photoionization cross sections have been computed for the Li-like to Fe-like ions of Ni. Level-resolved, Breit-Pauli  $R$ -matrix calculations were carried out for the Li-like to Na-like ions. Term-resolved  $R$ -matrix calculations were performed for Mg-like to Ca-like where the mass-velocity and Darwin relativistic corrections are included. Distorted wave calculations for Sc-like to Fe-like Ni were performed using AUTOSTRUCTURE where resonances are included using the isolated resonance approximation.

---

<sup>2</sup><http://heasarc.gsfc.nasa.gov/xstar/xstar.html>

<sup>3</sup><http://heasarc.gsfc.nasa.gov/uadb>

For all of the  $R$ -matrix calculations, total photoabsorption and total/partial photoionization data are available. Radiation and Auger dampings are included to account for radiation losses and the spectator Auger process. No damping is included for the AUTOSTRUCTURE calculations so we present only total photoabsorption cross sections which are convolved with a Gaussian profile using a width representative of currently deployed X-ray detectors.

We find overall good agreement with the background cross sections given by Verner & Yakovlev (1995), but our positions of the K edge are typically 40-80 eV higher. For Li-like Ni, we are in good agreement with Nahar (2005) as to resonance positions. However, we find much stronger resonant enhancement due to the finer energy mesh used in the present work.

All data are provided as on-line tables accompanying this article and can also be obtained through the XSTAR atomic database (Bautista & Kallman 2001) and the Universal Atomic Database. The data sets provided here together with the energy levels and radiative and Auger rates reported in Palmeri et al. (2008b) will help modelers to carry out detailed studies of K spectra of Ni ions.

Support for this research was provided in part by a grant from the NASA Astronomy and Physics Research (APRA) program. PP and PQ are respectively Research Associate and Senior Research Associate of the Belgian F.R.S.-FNRS. Financial support from this organization is acknowledged.

## REFERENCES

- Badnell, N. R. 1986, *J. Phys. B: At. Mol. Opt. Phys.*, 19, 3827
- . 1997, *J. Phys. B: At. Mol. Opt. Phys.*, 30, 1
- Bautista, M. A., & Kallman, T. R. 2001, *ApJS*, 134, 139
- Bautista, M. A., Mendoza, C., Kallman, T. R., & Palmeri, P. 2003, *A&A*, 403, 339
- . 2004, *A&A*, 418, 1171
- Berrington, K. A., Burke, P. G., Butler, K., Seaton, M. J., Storey, P. J., Taylor, K. T., & Yan, Y. 1987, *J. Phys. B: At. Mol. Opt. Phys.*, 20, 6379
- Berrington, K. A., Burke, P. G., Chang, J. J., Chivers, A. T., Robb, W. D., & Taylor, K. T. 1974, *Comput. Phys. Commun.*, 8, 149
- Berrington, K. A., Burke, P. G., Le Dourneuf, M., Robb, W. D., Taylor, K. T., & Ky Lan, V. 1978, *Comput. Phys. Commun.*, 14, 367
- Berrington, K. A., Eissner, W. B., & Norrington, P. H. 1995, *Comput. Phys. Commun.*, 92, 290
- Brenneman, L. W., et al. 2011, ArXiv e-prints
- Burke, P. G., Hibbert, A., & Robb, W. D. 1971, *J. Phys. B: At. Mol. Opt. Phys.*, 4, 153
- Burke, P. G., & Seaton, M. J. 1971, *Methods in Computational Physics*, Vol. 10, *Numerical Solution of the Integro-Differential Equations of Electron-Atom Collision Theory* (Academic Press), 1
- García, J., Mendoza, C., Bautista, M. A., Gorczyca, T. W., Kallman, T. R., & Palmeri, P. 2005, *ApJS*, 158, 68

- García, J., et al. 2009, *ApJS*, 185, 477
- Gorczyca, T. W., & Badnell, N. R. 1996, *J. Phys. B: At. Mol. Opt. Phys.*, 29, L283
- . 2000, *J. Phys. B: At. Mol. Opt. Phys.*, 33, 2511
- Hasoglu, M. F., Abdel-Naby, S. A., Gorczyca, T. W., Drake, J. J., & McLaughlin, B. M. 2010, *ApJ*, 724, 1296
- Kallman, T., & Bautista, M. 2001, *ApJS*, 133, 221
- Kallman, T. R., Bautista, M. A., Goriely, S., Mendoza, C., Miller, J. M., Palmeri, P., Quinet, P., & Raymond, J. 2009, *ApJ*, 701, 865
- Kallman, T. R., Palmeri, P., Bautista, M. A., Mendoza, C., & Krolik, J. H. 2004, *ApJS*, 155, 675
- Kanter, E. P., Dunford, R. W., Krässig, B., Southworth, S. H., & Young, L. 2006, *Radiat. Phys. Chem.*, 75, 2174
- Koyama, K. 2011, in *Astronomical Society of the Pacific Conference Series*, Vol. 439, *Astronomical Society of the Pacific Conference Series*, ed. M. R. Morris, Q. D. Wang, & F. Yuan, 418–+
- McClintock, J. E., et al. 2011, *Classical and Quantum Gravity*, 28, 114009
- Mendoza, C., Kallman, T. R., Bautista, M. A., & Palmeri, P. 2004, *A&A*, 414, 377
- Miller, J. M., Raymond, J., Fabian, A., Steeghs, D., Homan, J., Reynolds, C., van der Klis, M., & Wijnands, R. 2006, *Nature*, 441, 953
- Müller, A., et al. 2009, *J. Phys. B: At. Mol. Opt. Phys.*, 42, 235602
- . 2010, *J. Phys. B: At. Mol. Opt. Phys.*, 43, 135602

- Nahar, S. N. 2005, *ApJS*, 158, 80
- Palmeri, P., Mendoza, C., Kallman, T. R., & Bautista, M. A. 2003a, *A&A*, 403, 1175
- Palmeri, P., Mendoza, C., Kallman, T. R., Bautista, M. A., & Meléndez, M. 2003b, *A&A*, 410, 359
- Palmeri, P., Quinet, P., Mendoza, C., Bautista, M. A., García, J., & Kallman, T. R. 2008a, *ApJS*, 177, 408
- Palmeri, P., Quinet, P., Mendoza, C., Bautista, M. A., García, J., Witthoeft, M. C., & Kallman, T. R. 2008b, *ApJS*, 179, 542
- Ralchenko, Y., Kramida, A. E., Reader, J., & NIST ASD Team. 2008, NIST Atomic Spectra Database (version 4.0) (National Institute of Standards and Technology, Gaithersburg, MD), <http://physics.nist.gov/asd3>
- Robicheaux, F., Gorczyca, T. W., Pindzola, M. S., & Badnell, N. R. 1995, *Phys. Rev. A: At. Mol. Opt. Phys.*, 52, 1319
- Scully, S. W. J., et al. 2005, *J. Phys. B: At. Mol. Opt. Phys.*, 38, 1967
- Serlemitsos, P. J., Smith, B. W., Boldt, E. A., Holt, S. S., & Swank, J. H. 1977, *ApJ*, 211, L63
- Tamagawa, T. 2010, in *American Institute of Physics Conference Series*, Vol. 1269, American Institute of Physics Conference Series, ed. I. Tanihara, H. J. Ong, A. Tamii, T. Kishimoto, T. Kajino, S. Kubono, & T. Shima, 137–143
- Tamura, T., et al. 2009, *ApJ*, 705, L62
- Testa, P., Drake, J. J., Ercolano, B., Reale, F., Huenemoerder, D. P., Affer, L., Micela, G., & Garcia-Alvarez, D. 2008, *ApJ*, 675, L97

Veigele, W. J. 1973, *At. Data Nucl. Data Tables*, 5, 51

Verner, D. A., & Yakovlev, D. G. 1995, *A&AS*, 109, 125

Witthoeft, M. C., Bautista, M. A., Mendoza, C., Kallman, T. R., Palmeri, P., & Quinet, P.  
2009, *ApJS*, 182, 127

Witthoeft, M. C., García, J., Kallman, T. R., Bautista, M. A., Mendoza, C., Palmeri, P., &  
Quinet, P. 2011, *ApJS*, 192, 7

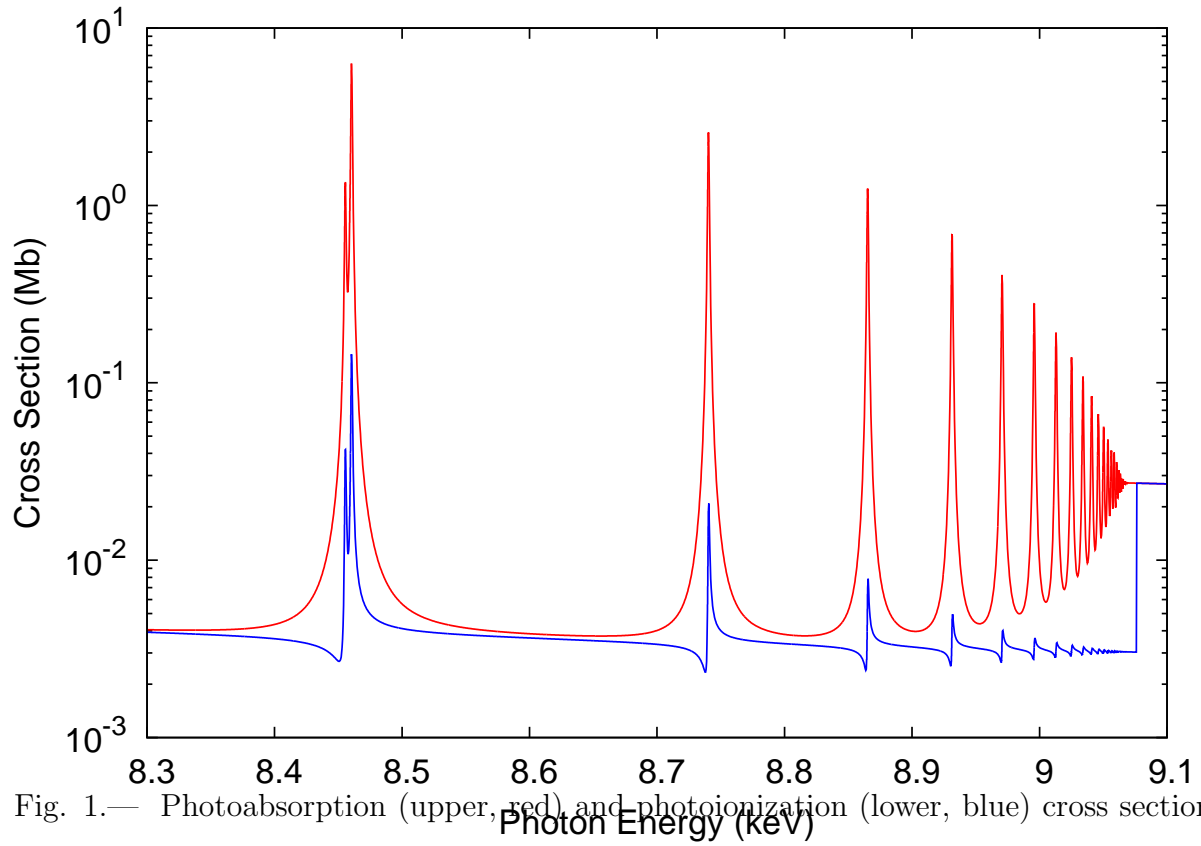


Fig. 1.— Photoabsorption (upper, red) and photoionization (lower, blue) cross sections of Ne-like Ni near the K edge. Color available in the on-line version of the text.

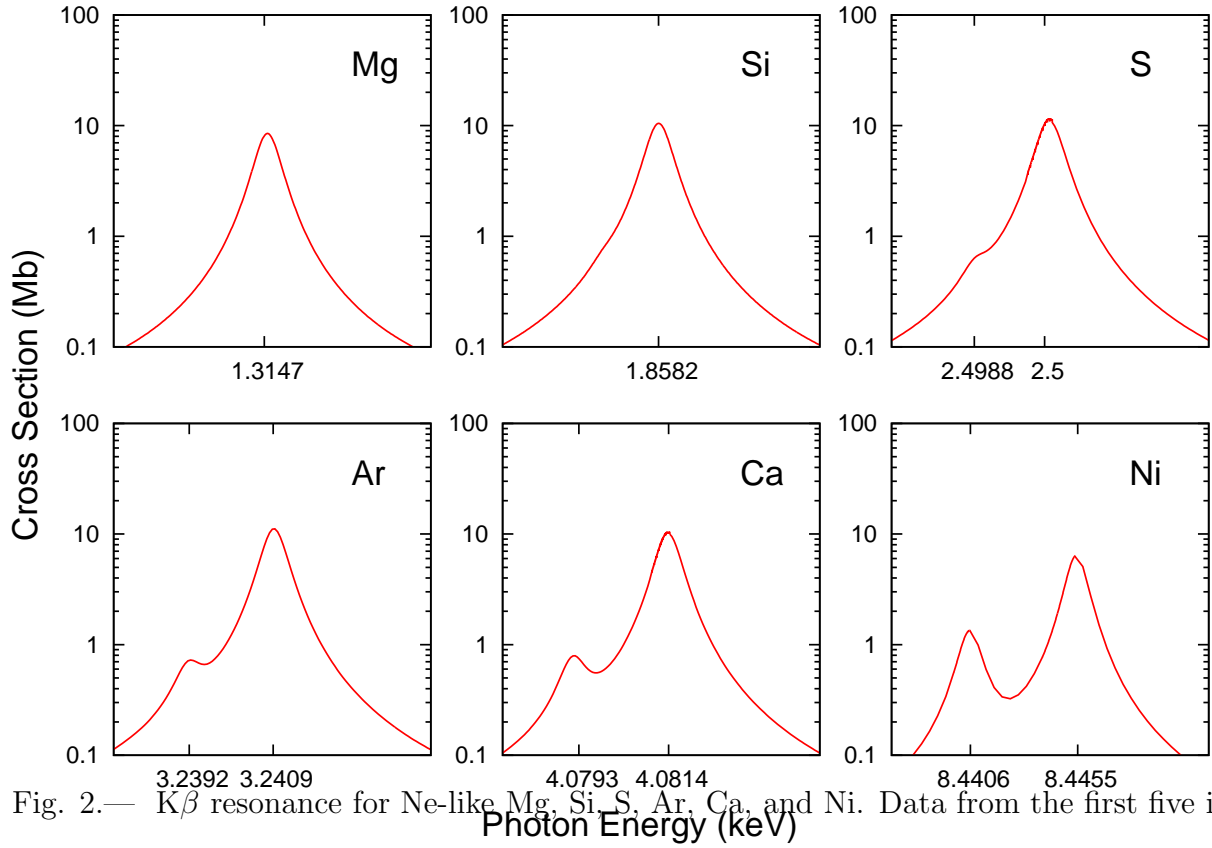


Fig. 2.—  $K\beta$  resonance for Ne-like Mg, Si, S, Ar, Ca, and Ni. Data from the first five ions comes from Witthoef et al. (2009). The second resonance appearing from Ne-like S to Ni is due to photoexcitation to the  $1s\ 2s^2\ 2p^6\ 3p\ ^3P_1$  level.

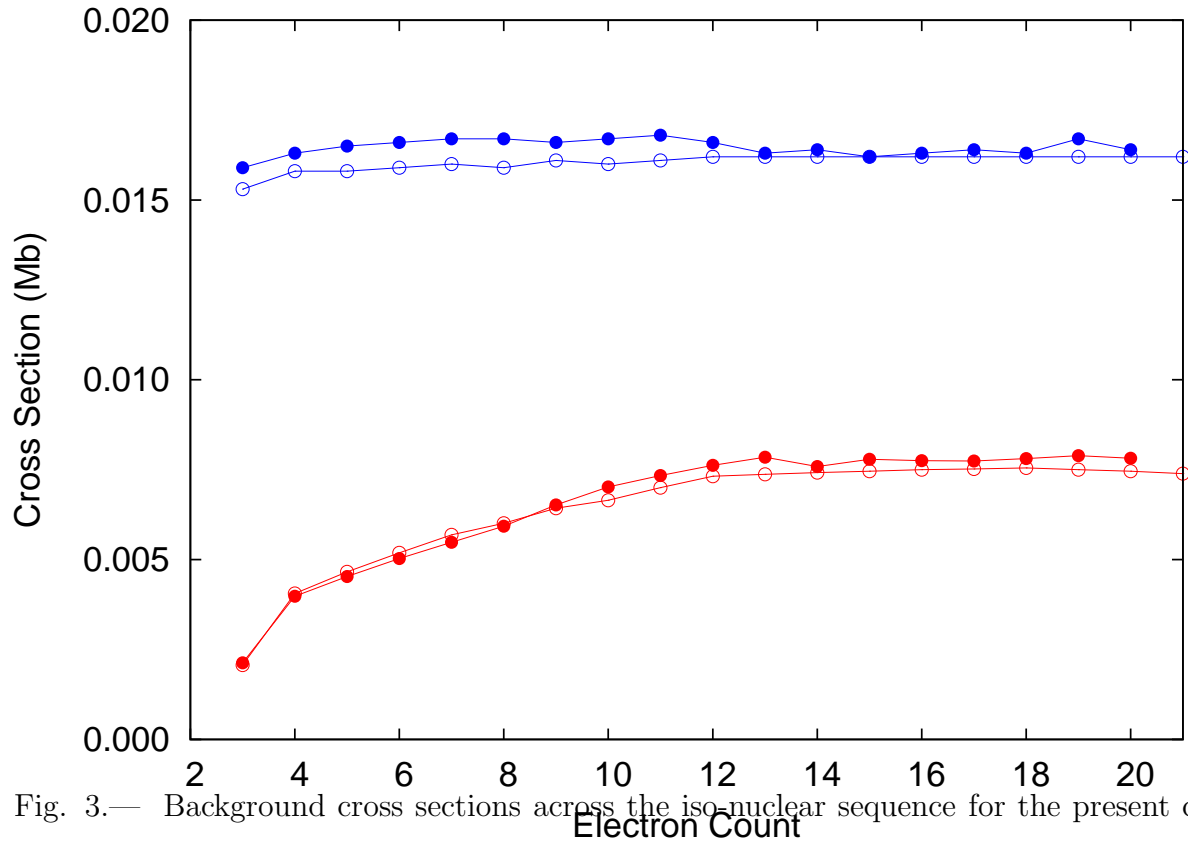


Fig. 3.— Background cross sections across the iso-nuclear sequence for the present calculations (filled circles) and Verner & Yakovlev (1995) (open circles). The upper two curves (blue) show the cross section above the K edge at 10.9 keV; lower two curves (red) give the cross section below the K edge at 6.8 keV. Color available in the on-line version of the text.

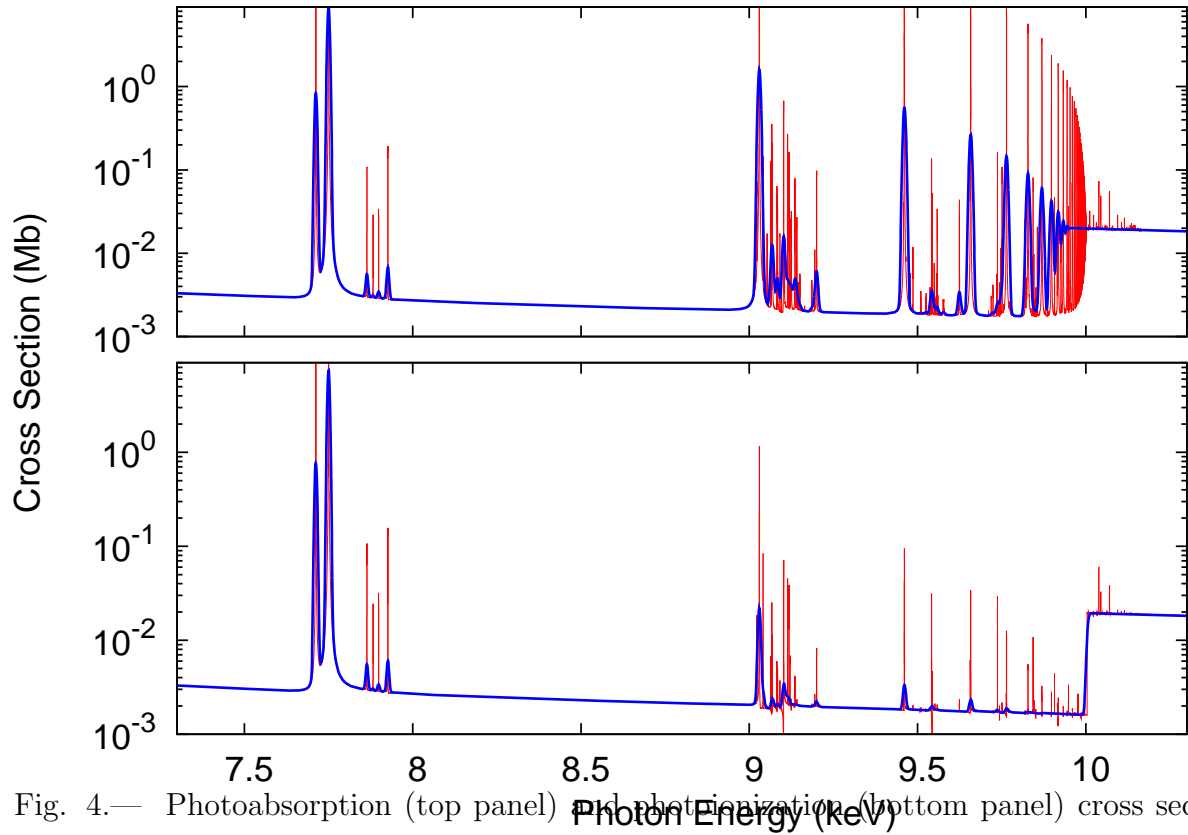


Fig. 4.— Photoabsorption (top panel) and partial photoionization (bottom panel) cross sections for Be-like Ni. Red, thin curves show the raw cross section and the blue, thick curves give the convolution with a Gaussian having a width of  $\Delta E/E = 10^{-4}$ . Color available in the on-line version of the text.

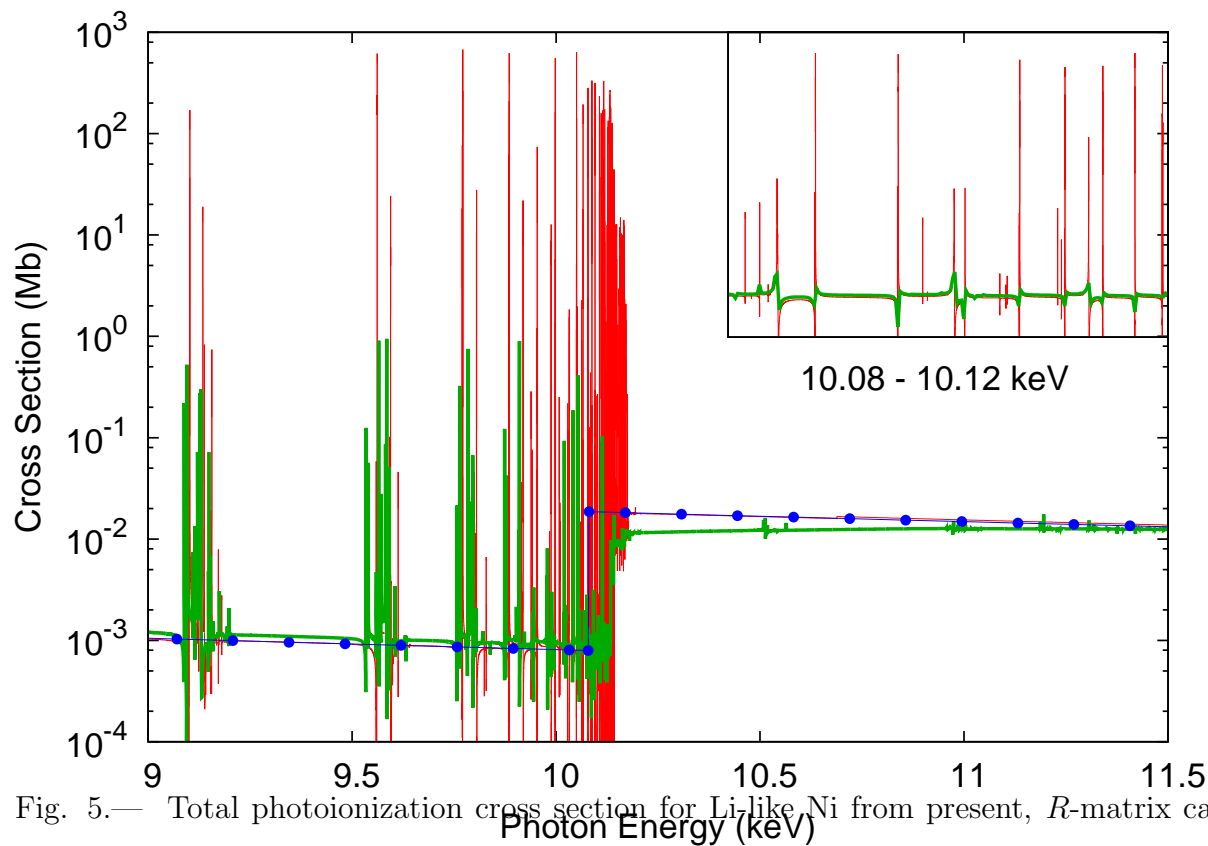


Fig. 5.— Total photoionization cross section for Li-like Ni from present, *R*-matrix calculation (thin, red curve), the *R*-matrix calculation of Nahar (2005) (thick, green curve), and Verner & Yakovlev (1995) (thin, blue curve with circles). The  $K\alpha$  resonances are not visible in this energy range. The background cross sections of Verner & Yakovlev (1995) are in excellent agreement with the present work. Inset: close-up of cross sections between 10.08 and 10.12 keV; range of cross sections is from  $10^{-4}$  to  $10^3$ . In the inset only, the Nahar (2005) cross sections have been shifted by 8.8 eV to align the resonance positions. Color available in the on-line version of the text.

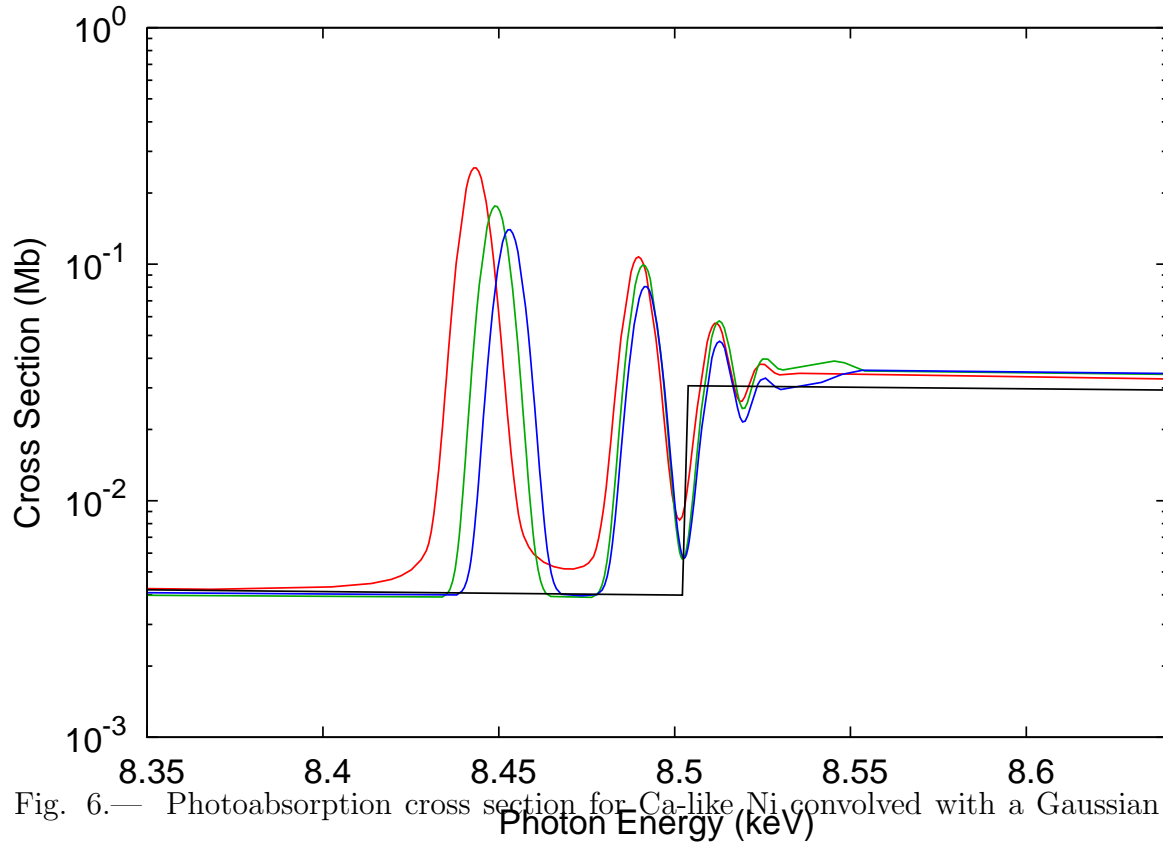


Fig. 6.— Photoabsorption cross section for Ca-like Ni convolved with a Gaussian having a width of  $\Delta E/E = 10^{-3}$ . Based on the height of the resonance feature near 8.45 keV, in order from strongest to weakest, the curves are: *R*-matrix results (red), AUTOSTRUCTURE using target wave functions (green), AUTOSTRUCTURE using parent wave functions (blue), and the background cross section of Verner & Yakovlev (1995) (black). Color available in the on-line version of the text.